JOC*Article*

Spin Trapping by 5-Carbamoyl-5-methyl-1-pyrroline *N*-Oxide (AMPO): Theoretical and Experimental Studies

Frederick A. Villamena,*,† Antal Rockenbauer,§ Judith Gallucci,‡ Murugesan Velayutham,† Christopher M. Hadad,*,‡ and Jay L. Zweier*,†

Center for Biomedical EPR Spectroscopy and Imaging, The Davis Heart and Lung Research Institute, and the Division of Cardiovascular Medicine, Department of Internal Medicine, College of Medicine, and the Department of Chemistry, The Ohio State University, Columbus, Ohio 43210, and Chemical Research Center, Institute of Chemistry, H-1025 Budapest, Pusztaszeri 59, Hungary

villamena-1@medctr.osu.edu; hadad.1@osu.edu; zweier-1@medctr.osu.edu

Received May 4, 2004

The nitrone 5-carbamoyl-5-methyl-1-pyrroline *N*-oxide (AMPO) was synthesized and characterized. Spin trapping of various radicals by AMPO was demonstrated for the first time by electron paramagnetic resonance (EPR) spectroscopy. The resulting spin adducts for each of these radicals gave unique spectral profiles. The hyperfine splitting constants for the superoxide adduct are as follows: isomer I (80%), $a_{\text{nitronyl-N}} = 13.0$ G and $a_{\beta\text{-H}} = 10.8$ G; isomer II (20%), $a_{\text{nitronyl-N}} = 13.1$ G, $a_{\beta\text{-H}} = 12.5$ G, and $a_{\gamma\text{-H}} = 1.75$ G. The half-life of the AMPO$-O_2$H was about 8 min, similar to that observed for EMPO but significantly shorter than that of the DEPMPO$-O_2$H with $t_{1/2} \sim 16$ min. However, the spectral profile of AMPO$-O_2$H at high S/N ratio is distinguishable from the spectrum of the $^{\bullet}$OH adduct. Theoretical analyses using density functional theory calculations at the B3LYP/6-31+G**//B3LYP/6-31G* level were performed on AMPO and its corresponding superoxide adduct. Calculations predicted the presence of intramolecular H-bonding in both AMPO and its superoxide adduct. The H-bonding interaction was further confirmed by an X-ray structure of AMPO, and of the novel and analogous amido nitrone 2-amino-5-carbamoyl-5-methyl-1-pyrroline *N*-oxide (NH_2–AMPO). The thermodynamic quantities for superoxide radical trapping by various nitrones have been found to predict favorable formation of certain isomers. The measured partition coefficient in an *n*-octanol/buffer system of AMPO was similar to those of DMPO and DEPMPO. This study demonstrates the suitability of the AMPO nitrone for use as a spin trap to study radical production in aqueous systems.

Introduction

Spin trap development has been a major focus in free radical research and is of great importance for the measurement of free radicals in chemical and biological systems. Spin trapping by electron paramagnetic resonance (EPR) spectroscopy has been widely employed to detect radical adducts with high sensitivity and specificity.[1–3] There are generally two families of spin traps, the linear or PBN-type and the cyclic or DMPO-type nitrones.

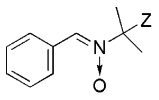

PBN-type

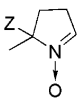

DMPO-type

Several PBN-type nitrones have been synthesized such as the α-substituted methoxy, amino, cyano, and mercapto nitrones,[4,5] as well as the alkoxy-phosphoryl[6] and -carboxyl[7] derivatives, but the DMPO-type analogues are by far the most commonly used. These DMPO-type spin traps include the alkoxyphosphorylated nitrones 5-diethoxyphosphoryl-5-methyl-1-pyrroline *N*-oxide (DEPMPO)[8–10] and 5-diisopropyloxyphosphoryl-5-methyl-1-pyrroline *N*-oxide (DIPPMPO),[11] and the alkoxycarbonyl nitrones 5-ethoxycarbonyl-5-methyl-1-pyrroline *N*-oxide (EMPO)[12–15] and 5-butoxycarbonyl-5-methyl-1-pyrroline *N*-oxide (Boc-MPO).[15–18] These substituted DMPO-type nitrones have

* Address correspondence to these authors. F.A.V.: fax (614)-292-8454. C.M.H.: fax (614)-292-1685. J.L.Z.: fax: (614)-247-7799.

† Center for Biomedical EPR Spectroscopy and Imaging, The Davis Heart and Lung Research Institute, College of Medicine, The Ohio State University.

§ Chemical Research Center, Institute of Chemistry.

‡ Department of Chemistry, The Ohio State University.

(1) Rosen, G. M.; Cohen, M. S.; Britigan, B. E.; Pou, S. *Free Radical Res. Commun.* **1990**, *9*, 187–195.

(2) Rhodes, C. J. *Toxicology of the Human Environment*; Taylor and Francis Ltd.: London, UK, 2000.

(3) Rosen, G. M.; Britigan, B. E.; Halpern, H. J.; Pou, S. *Free Radicals*: *Biology and Detection by Spin Trapping*; Oxford University Press: New York, 1999.

(4) Acken, B. J.; Gallis, D. E.; Warshaw, J. A.; Crist, D. R. *Can. J. Chem.* **1992**, *70*, 2076–2080.

(5) Gallis, D. E.; Warshaw, J. A.; Acken, B. J.; Crist, D. R. *Collect. Czech. Chem. Commun.* **1993**, *59*, 125–141.

(6) Zeghdaoui, A.; Tuccio, B.; Finet, J.-P.; Cerri, V.; Tordo, P. *J. Chem. Soc., Perkin Trans. 2* **1995**, *12*, 2087–2089.

(7) Allouch, A.; Roubaud, V.; Lauricella, R.; Bouteiller, J.-C.; Tuccio, B. *Org. Biomol. Chem.* **2003**, *1*, 593–598.

(8) Frejaville, C.; Karoui, H.; Tuccio, B.; Le Moigne, F.; Culcasi, M.; Pietri, S.; Lauricella, R.; Tordo, P. *J. Med. Chem.* **1995**, *38*, 258–265.

(9) Liu, K. J.; Miyake, M.; Panz, T.; Swartz, H. *Free Radical Biol. Med.* **1999**, *26*, 714–721.

(10) Stolze, K.; Udilova, N.; Nohl, H. *Free Radical Biol. Med.* **2000**, *29*, 1005–1014.

10.1021/jo049244i CCC: $27.50
Published on Web 10/19/2004

demonstrated a relatively higher rate of superoxide ($O_2^{\bullet -}$) trapping and the corresponding $O_2^{\bullet -}$ adducts have longer half-lives as compared to that of DMPO. Although the spin trapping capabilities of both the PBN and DMPO-type nitrones have been demonstrated, they have certain critical limitations. PBN-type nitrones are limited by their ability to discern different radicals, while the DMPO-type nitrones are limited by the stability of the adducts formed and the overall spin trapping efficiency.

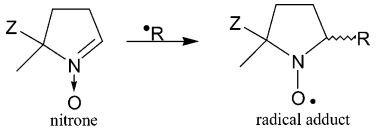

nitrone radical adduct

nitrone	Z
HMPO	-H
DMPO	-Me
EMPO	-CO_2Et
BocMPO	-CO_2t-Bu
DEPMPO	-P(O)(OEt)$_2$
DIPPMPO	-P(O)(O*i*-Pr)$_2$

In our previous studies, we explored how theoretical analysis can provide insights into the spin trapping properties and spin adduct stability of nitrones and their corresponding nitroxyl spin adducts, respectively.[16,19] On the basis of our recent theoretical studies with a density functional theory approach, we showed that 5-carbamoyl-5-methyl-1-pyrroline *N*-oxide (AMPO)[20] and its spin adduct (AMPO−OH) have similar electronic and thermodynamic properties compared to the phosphorylated and carboxylated nitrones and their adducts. This comparison, therefore, motivated us to explore the spin trapping characteristics of AMPO. The compound AMPO

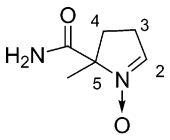

AMPO

has been previously synthesized[21] as a model system to study the oxidation of hydroxyamino-amide, but it has not been evaluated as a spin trap. For the first time, we now report the spin trapping and spin adduct characteristics of AMPO.

Results and Discussion

Theoretical Analysis. Figure S19 shows the naming system used in this study while Table S15 gives the pertinent dihedral angles in each $^{\bullet}O_2H$ adduct. The N−O and C=N bond distances for all nitrones are in the range of 1.25−1.27 and 1.30−1.31 Å, respectively, consistent with previously reported experimental data of 1.294(1)[22] and 1.307(2) Å[23] for N−O and C=N bonds, respectively. The X-ray structure of AMPO shows bond distances of 1.310(2) Å for N−O and 1.286(2) Å for the C=N bond. The preferred B3LYP/6-31G* geometry for AMPO is the Newman projection shown here and in Figure 1 (top) in

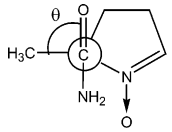

AMPO

which the carbonyl oxygen is oriented opposite to the N−O direction. Optimization attempts with different initial starting conformations only gave the same conformation. The calculated dihedral angle for $\angle CH_3-C-CNH_2-O$ was $\theta = 99.4°$ and for NH_2-AMPO ∠C6−C1−C5−O2 = 90.1(2)°. The range of nitroxyl N−O bond distances is 1.28−1.34 Å, comparable to the experimental value of 1.267 (5) Å[23] for 2,2,5,5-tetramethyl-3-carbamidopyrroline-l-oxyl (TMCO).

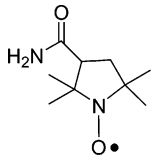

TMCO

Natural population analysis revealed that spin densities on the isolated $HOO^{\bullet}$ radical shows 73% distribution on the terminal O while 27% on the internal O. The average spin densities within the N−O moiety in the radical adducts are 39% and 56% on the N and O atoms, respectively. The O−O bond distance in the free $HOO^{\bullet}$ radical is shorter, i.e., 1.33 Å, compared to the O−O bond distance in the $^{\bullet}O_2H$ adducts, which has a mean average of 1.455 (2) Å, similar to that observed in **1** of 1.4599(17) Å.[24]

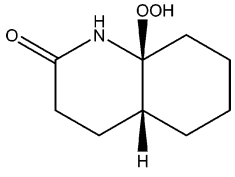

1

Since the pK_a of $HOO^{\bullet}$ is approximately 4.8,[25] it could certainly be assumed that the attacking species is $O_2^{\bullet -}$ at neutral pH.[26,27] Therefore, we explored the most

(11) Chalier, F.; Tordo, P. *J. Chem. Soc., Perkin Trans. 2* **2002**, 2110−2117.
(12) Olive, G.; Mercier, A.; Le Moigne, F.; Rockenbauer, A.; Tordo, P. *Free Radical Biol. Med.* **2000**, *28*, 403−408.
(13) Zhang, H.; Joseph, J.; Vasquez-Vivar, J.; Karoui, H.; Nsanzumuhire, C.; Martasek, P.; Tordo, P.; Kalyanaraman, B. *FEBS Lett.* **2000**, *473*, 58−62.
(14) Stolze, K.; Udilova, N.; Nohl, H. *Biol. Chem.* **2002**, *383*, 813−820.
(15) Stolze, K.; Udilova, N.; Rosenau, T.; Hofinger, A.; Nohl, H. *Biol. Chem.* **2003**, *384*, 493−500.
(16) Villamena, F.; Zweier, J. *J. Chem. Soc., Perkin Trans. 2* **2002**, 1340−1344.
(17) Zhao, H.; Joseph, J.; Zhang, H.; Karoui, H.; Kalyanaraman, B. *Free Radical Biol. Med.* **2001**, *31*, 599−606.
(18) Tsai, P.; Ichikawa, K.; Mailer, C.; Pou, S.; Halpern, H. J.; Robinson, B. H.; Nielsen, R.; Rosen, G. M. *J. Org. Chem.* **2003**, *68*, 7811−7817.
(19) Villamena, F.; Hadad, C. M.; Zweier, J. *J. Phys. Chem. A* **2003**, *107*, 4407−4414.
(20) Villamena, F.; Hadad, C. M.; Zweier, J. *J. Am. Chem. Soc.* **2004**, *126*, 1816−1829.
(21) Alderson, G. W.; Black, D. S.; Clark, V. M.; Todd, L. *J. Chem. Soc., Perkin Trans. 1* **1976**, 1955−1960.

SCHEME 1. Possible Mechanisms for Formation of the AMPO−O_2H with Free Energies of Reaction $\Delta G_{Rxn,298K}$ (kcal/mol) in the Gas Phase at the B3LYP/6-31+G//B3LYP/6-31G* Level[a]**

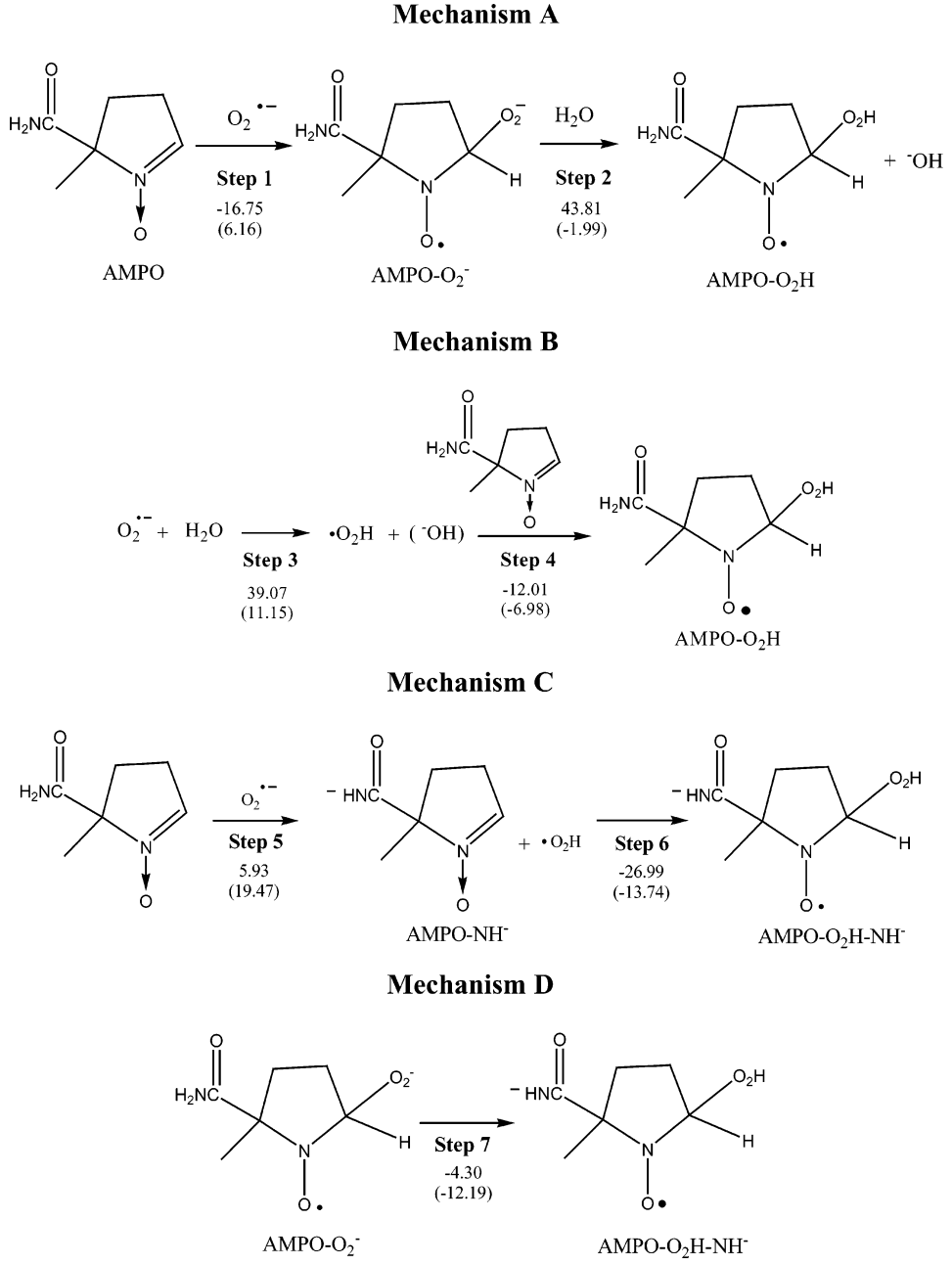

[a] Values in parentheses are in the aqueous phase at the B3LYP/6-31+G**(PCM)//B3LYP/6-31G* level of theory.

favorable route for superoxide adduct formation using computational methods as shown in Scheme 1 with the corresponding reaction free energies ($\Delta G_{298K,rxn}$ in kcal/mol) for each step both in gaseous and aqueous phases (using the PCM model for water). Several conformational as well as configurational isomers have been considered in the approximation of the energetics of each of the reaction steps, and the $\Delta G_{298K,rxn}$ values only reflect the energy difference for the most thermodynamically favored isomer of reactants and products (see Supporting Information Tables S19, S20, and S22 for the structures and thermodynamic parameters of these isomers).

Once $O_2^{\bullet-}$ is formed in solution, it could add directly to the nitrone (step 1), undergo protonation (step 3), or abstract a proton from an amide group (step 5). Steps 3 and 5 gave endoergic gas-phase ΔG_{rxn} values of 39.07 and 5.93 kcal/mol compared to an exoergic value of −16.75 kcal/mol for step 1. Mechanism B should only occur at acidic pH given that the pK_a of water and $RCONH_2$ are

(22) Villamena, F. A.; Dickman, M. H.; Crist, D. R. *Inorg. Chem.* **1998**, *37*, 1446−1453.
(23) Turley, J. W.; Boer, F. P. *Acta Crystallogr.* **1972**, *B28*, 1641−1644.
(24) Alini, S.; Citterio, A.; Farina, A.; Fochi, M. C.; Malpezzi, L. *Acta Crystallogr.* **1998**, *C54*, 1000−1003.
(25) Bielski, B. H. J. *Photochem. Photobiol.* **1978**, *28*, 645−649.
(26) Halliwell, B.; Gutteridge, J. M. C. In *Free Radicals in Biology and Medicine*; Oxford Univeristy Press: Oxford, UK, 1999; pp 60−61.
(27) Finkelstein, E.; Rosen, G. M.; Rauckman, E. J. *J. Am. Chem. Soc.* **1980**, *102*, 4995.

about 15.75 and 25,[28] respectively, and that HOO• is relatively acidic at 25 °C. Mechanism A, therefore, seems to be the most plausible route for superoxide adduct formation, in which $O_2^{\bullet-}$ is predominant in solution and its addition to AMPO yields the AMPO−O_2^-, which is subsequently protonated to yield the hydroperoxyl adduct, AMPO−O_2H. Although the proton abstraction processes in steps 2 and 3 are both endoergic in the gas phase (43.81 and 39.07 kcal/mol, respectively), formation of AMPO−O_2H from the AMPO−O_2^- and H_2O (step 2) may be possible in H_2O due to more favorable thermodynamic parameters when compared to the direct formation of HOO• from $O_2^{\bullet-}$ and H_2O (step 3). This is further supported by the experimental pK_a reported for various alkyl hydroperoxides in water at 25 °C, which is in the range of 11.65−12.8.[29] Moreover, experimental evidence shows that the addition of $O_2^{\bullet-}$ to 5-*tert*-butoxycarboxy-5-methyl-1-pyrroline *N*-oxide at various pH values has been reported to be relatively slower at pH 7.0 with k_{app} = 75.0 M^{-1} s^{-1} compared to k_{app} = 239.2 M^{-1} s^{-1} at pH 5.0.[18] This difference in rate constants at various pH values further supports that $O_2^{\bullet-}$ dominates in neutral pH while HOO• is formed at acidic pH, and correlates well with the experimental reduction potentials of $E°$ = 1.06 and 0.94 V for HOO• and $O_2^{\bullet-}$, respectively, demonstrating their relative reactivity.[30] Mechanism D shows the possibility of intramolecular proton abstraction of the amide proton by the superoxide moiety. Although step 7 is exoergic, ΔG_{rxn} = −12.19 kcal/mol in the aqueous phase, typical pK_a values for $RCONH_2$ of 25[28] and ROOH of 11.65−12.8[29] would indicate that the equilibrium should favor reactants over the products; however, in this case, intramolecular hydrogen bonding biases the system to strongly favor the products.

Table 1 shows the enthalpy changes for the formation of various •O_2H adducts from the corresponding nitrones and HOO•. Examination of the thermodynamic quantities for trapping HOO• by various nitrones reveals that enthalpies of reaction are less exothermic, i.e., ΔH_{rxn} ∼ 18−29 kcal/mol exothermic (see Table 1), compared to the trapping of •OH, which was predicted to be on the order of ΔH_{rxn} ∼ 51−58 kcal/mol exothermic.[19,20] The most energetically preferred isomers are AMPO−O_2H *cis*-2a, EMPO−O_2H *cis*-1, and DEPMPO−O_2H *trans*-2. Analysis of all these optimized structures predicted the presence of intramolecular H-bonding, i.e., −OOH- - -O−N in all adducts and an additional −N−O- - -H−N bonding mode for AMPO−O_2H *cis*-2a (see Figure 1). Interestingly, the formation of DEPMPO−O_2H *cis*-3H with intramolecular H-bonding involving −P=O- - -H−OO− was predicted to be 2.7 kcal/mol less exothermic than DEPMPO−O_2H *trans*-2, contrary to the DEPMPO−OHs reported previously in which the presence of −P=O- - -H−O− in DEPMPO−OH *cis* stabilizes the adduct by 2.4 kcal/mol compared to DEPMPO−OH *trans*-2 adduct.[20]

On the basis of Table 1, it is apparent that the enthalpy changes for the formation of AMPO−O_2H, EMPO−O_2H, and DEPMPO−O_2H show less than 0.1 kcal/mol difference in the formation of cis adducts compared to formation of trans adducts. It is predicted that there are a lesser number of conformational and configurational isomers of AMPO−O_2H (Table 1) compared to EMPO−O_2H and DEPMPO−O_2H. However, assuming that the *g* values of individual isomers are the same, this prediction on the number of isomers was not observed as the experimental line widths among the $O_2^{\bullet-}$ adducts did not show any significant differences, i.e., EMPO−O_2H (2.3 G) and DEPMPO−O_2H (1.8 G) and AMPO−O_2H (2.3 G). Consistent with the EPR spectra for $O_2^{\bullet-}$ adducts of EMPO[12] and DEPMPO[8,31] (Figure 2), the lowest field peak is broadened, possibly due to the presence of diastereomeric mixtures of $O_2^{\bullet-}$ adducts.

Four isomers were predicted for AMPO−O_2H as shown in Figure 1 with different modes of intramolecular H-bonding, i.e., −N−O- - -H−N, −OOH- - -O=C, and −N−O- - -HOO−. The AMPO−O_2H *cis*-3 adduct has the shortest intramolecular H-bond distance of 1.90 Å on an OOH- - -O=C− bond motif, but it is not the most thermodynamically preferred isomer. A closer look at the spin density distribution on various AMPO−O_2H using natural population analysis indicate a 0.1−0.3% delocalization of spin on the amido-N compared to about 1.9−2.5% delocalization on the phosphoryl-P in the DEPMPO−O_2H (Table S16). In general, at least 1 γ-H in all adducts exhibit 0.1% spin density distribution while 0.8−2.0% was predicted for the β-H's. Values of isotropic hyperfine splitting constant a_X for the various adducts can be calculated from the nuclear spin density ρ_{rx} (Fermi

TABLE 1. Reaction Enthalpies ΔH_{rxn} (in kcal/mol) for the Formation of the Hydroperoxyl Adducts[a] at the B3LYP/6-31+G//B3LYP/6-31G* Level at 298 K**

spin adducts	ΔH_{rxn}	spin adducts	ΔH_{rxn}
HMPO		EMPO−O_2H *trans*-1	−24.16
HMPO−O_2H	−23.67	EMPO−O_2H *trans*-2	−23.24
DMPO		EMPO−O_2H *trans*-3	−26.23
DMPO−O_2H	−24.95	**DEPMPO-1**	
AMPO		DEPMPO−O_2H *cis*-1	−26.70
AMPO−O_2H *cis*-2a	−24.18[b]	DEPMPO−O_2H *cis*-2	−26.56
AMPO−O_2H *cis*-2b	−20.40	DEPMPO−O_2H *cis*-3	−23.09
AMPO−O_2H *cis*-3	−17.81	DEPMPO−O_2H *cis*-3H	−24.36
AMPO−O_2H *trans*-2	−23.55	DEPMPO−O_2H *trans*-1	−26.08
EMPO-1		DEPMPO−O_2H *trans*-2	−27.05[b]
EMPO−O_2H *cis*-1	−26.07[b]	DEPMPO−O_2H *trans*-3	−24.87
EMPO−O_2H *cis*-2	−21.68	**DEPMPO-2**	
EMPO−O_2H *cis*-3	−25.16	DEPMPO−O_2H *cis*-1	−28.57
EMPO−O_2H *trans*-1	−23.91	DEPMPO−O_2H *cis*-2	−28.42
EMPO−O_2H *trans*-2	−22.99	DEPMPO−O_2H *cis*-3	−24.96
EMPO−O_2H *trans*-3	−25.97	DEPMPO−O_2H *cis*-3H	−26.22
EMPO-2		DEPMPO−O_2H *trans*-1	−27.95
EMPO−O_2H *cis*-1	−25.88[b]	DEPMPO−O_2H *trans*-2	−28.91[b]
EMPO−O_2H *cis*-2	−21.48	DEPMPO−O_2H *trans*-3	−26.74
EMPO−O_2H *cis*-3	−24.97	**DEPMPO-3**	
EMPO−O_2H *trans*-1	−23.71	DEPMPO−O_2H *cis*-1	−24.57
EMPO−O_2H *trans*-2	−22.80	DEPMPO−O_2H *cis*-2	−24.43
EMPO−O_2H *trans*-3	−25.78	DEPMPO−O_2H *cis*-3	−20.96
EMPO-3		DEPMPO−O_2H *cis*-3H	−22.22
EMPO−O_2H *cis*-1	−26.32[b]	DEPMPO−O_2H *trans*-1	−23.95
EMPO−O_2H *cis*-2	−21.93	DEPMPO−O_2H *trans*-2	−24.92[b]
EMPO−O_2H *cis*-3	−25.42	DEPMPO−O_2H *trans*-3	−22.74

[a] See Figures S19 and Table S15 for the corresponding structure of the naming system used. [b] Most stable conformer.

(28) Gordon, A. J.; Ford, R. A., Eds. *The Chemist's Companion*: *A Handbook of Practical Data*, *Techniques*, *and References*; Wiley-Interscience: New York, 1972.
(29) Richardson, W. H.; Hodge, V. F. *J. Org. Chem.* **1970**, *35*, 4012−4016.
(30) Buettner, G. R. *Arch. Biochem. Biophys.* **1993**, *300*, 535−543.
(31) Barbati, S.; Clement, J. L.; Olive, G.; Roubaud, V.; Tuccio, B.; Tordo, P. In *Free Radicals in Biology*, *Environment*; Minisci, F., Ed.; Kluwer Academic Publishers: Dordrecht, The Netherlands, 1997; pp 39−47.

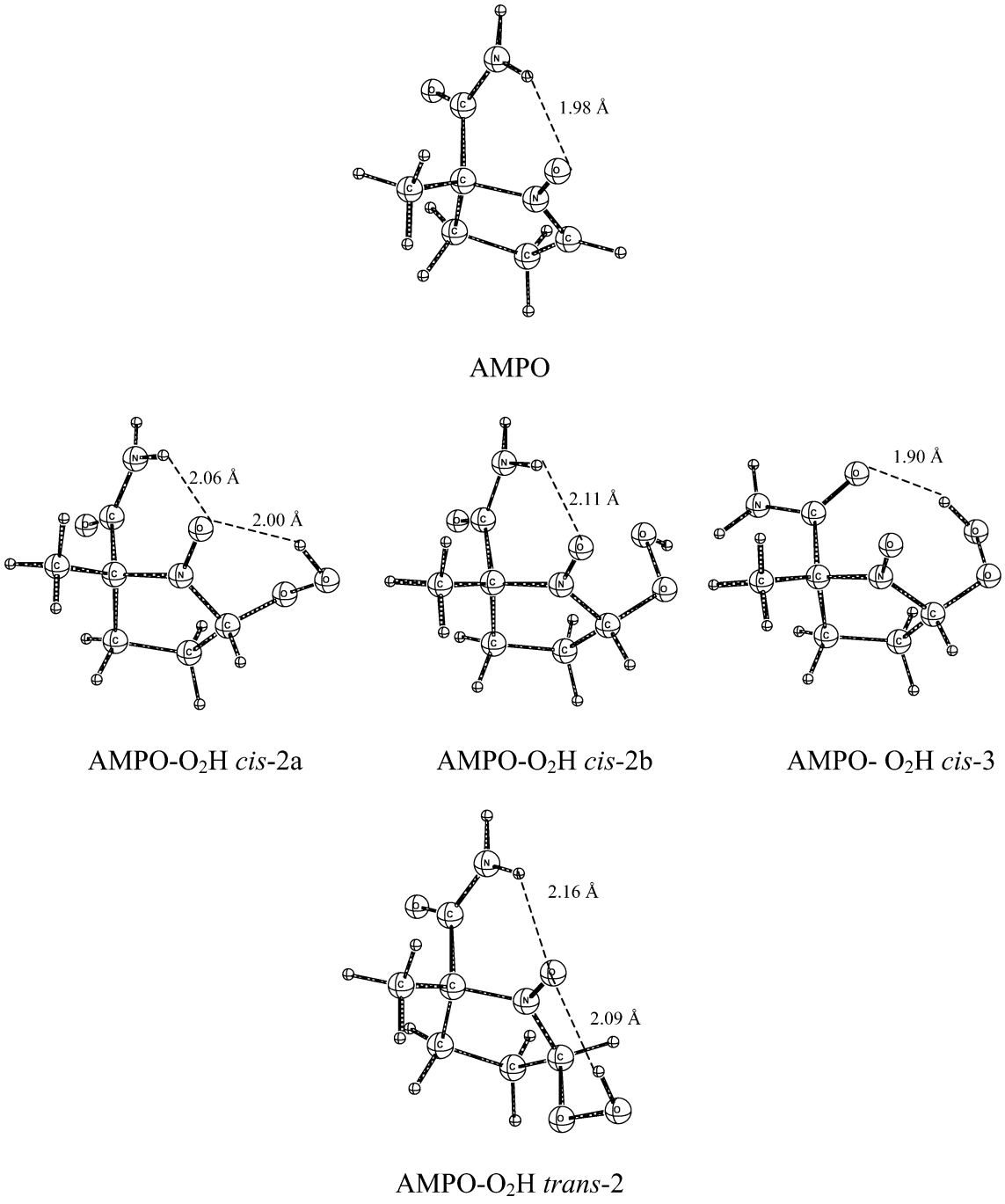

FIGURE 1. A view of the most stable B3LYP/6-31G* optimized structures of AMPO (top) and its superoxide adducts.

contact terms) based on eq 1, where g_0 is the isotropic

$$a_X = 8\pi/3(g_e/g_0)\gamma_X\beta_X\rho_{rx} \quad (1)$$

g-value for the radical, g_e the g-value for the free electron, γ_X the gyromagnetic nuclear ratio, and β_X the nuclear magneton of the nucleus X.[32] Although these small percentage values for the spin density distribution may seem insignificant, their corresponding a_X in Gauss (Table S17) could indeed give a significant influence on their spectral profiles as will be discussed later in the Spin Trapping section.

Structural Analysis. AMPO was synthesized from EMPO in the absence of NaCN catalyst and was fully characterized with spectroscopic techniques. One advantage of AMPO over commonly used nitrones such as DMPO, EMPO, and DEPMPO is that as a solid, its ease of purification makes AMPO less susceptible to contamination from paramagnetic impurities. ^{1}H NMR spectra of AMPO in D_2O show fast exchange of the amido H's while two nonequivalent amido H's in $CDCl_3$, relatively broad peaks at 5.43 and 8.25 ppm, indicate restricted NH_2 group rotation around the C−N bond. This could

(32) Cirujeda, J.; Vidal-Gancedo, J.; Jürgens, O.; Mota, F.; Novoa, J. J.; Rovira, C.; Veciana, J. *J. Am. Chem. Soc.* **2000**, *122*, 11393−11405.

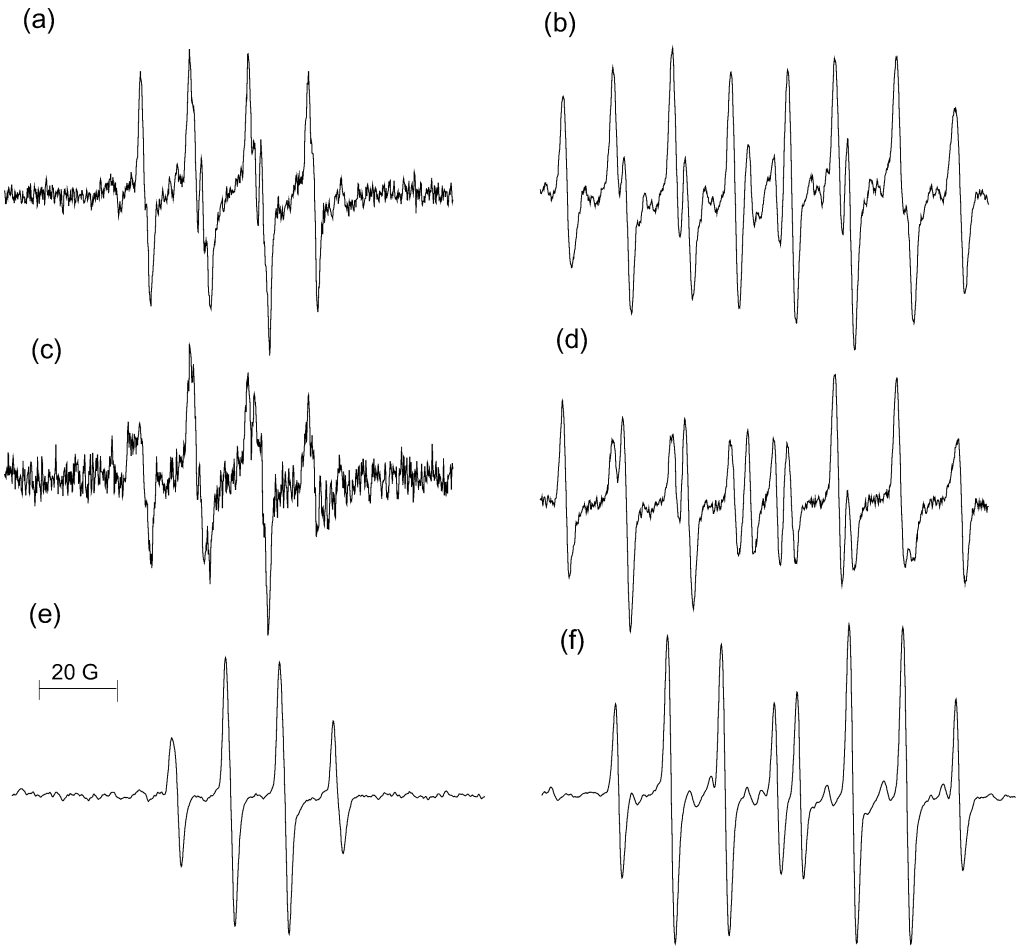

FIGURE 2. EPR spectral profile of EMPO−O_2H (a) and DEPMPO−O_2H (b) adducts after 5 min of irradiation, using the light-riboflavin system to generate $O_2^{\bullet-}$ and (c and d) spectra of the same adducts, respectively, taken 1 h after the light was turned off; (e and f) spectra of EMPO−OH and DEPMPO−OH, using the Fenton reaction, respectively. See experimental methods for spectrometer settings.

be partly due to intramolecular H-bonding of the NH_2 with the nitronyl O.

It was worth investigating the X-ray structures of AMPO and NH_2−AMPO since these experimental data can provide important structural information for nitrones with an amido substituent. The compound NH_2−AMPO was produced from aminolysis of the carbonyl C and a series of reactions involving an oxidation of the nitrone functionality as facilitated by the initial nucleophilic substitution by CN^- (Scheme 2). X-ray crystallographic structures for AMPO and NH_2−AMPO are shown in Figure 3.

Theoretical analysis of AMPO predicted intramolecular H-bonding of amido H with nitronyl O giving a bond distance of 1.98 Å (Figure 1, top). The X-ray packing arrangement for AMPO shown in Figure 4 indicates intermolecular H-bonding of the amido H with the nitronyl O with bond distances of 1.95 and 2.15 Å, respectively, while the novel nitrone NH_2−AMPO exhibited both inter- and intramolecular H-bonding of the amide moiety to the nitronyl O with distances of 1.96 and 2.10 Å (see Supporting Information). Crystallographic details of the compounds AMPO and NH_2−AMPO are shown in the Supporting Information as Tables S1−S6 and Tables S7−S14, respectively.

SCHEME 2. Synthesis of AMPO and NH_2−AMPO

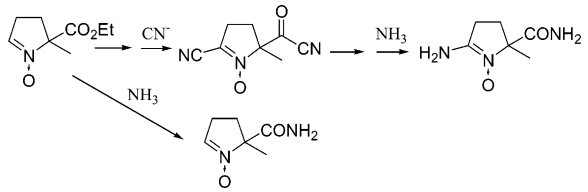

Spin Trapping. The addition of various radicals to AMPO was performed in a phosphate buffer and characteristic spectral profiles were observed for each of the adducts (Figure 5). Table 2 shows a summary of all of the observed EPR spectral parameters. Although the overall spectral profile for the $^{\bullet}$OH, *t*-Bu$O^{\bullet}$, and glutathionyl (G$S^{\bullet}$) adducts are similar, their hyperfine splitting constant (hfsc) assignments vary. The superoxide adduct of AMPO gave a spectral profile (Figure 6a,b) similar to those observed for DMPO and alkoxycarboxylated O_2H adducts. The AMPO−O_2H generated from xanthine-xanthine oxidase, PMA activated neutrophils, or riboflavin-light systems (see Figures 6 and 7) gave hyperfine splittings resulting from a mixture of two diastereomers and simulation of these spectra gave hfsc assignments for isomer I (80%) of $a_{\text{nitronyl-N}} = 13.0$ G and $a_{\beta\text{-H}} = 10.8$ G and for isomer II (20%) $a_{\text{nitronyl-N}} = 13.1$ G, $a_{\beta\text{-H}} = 12.5$

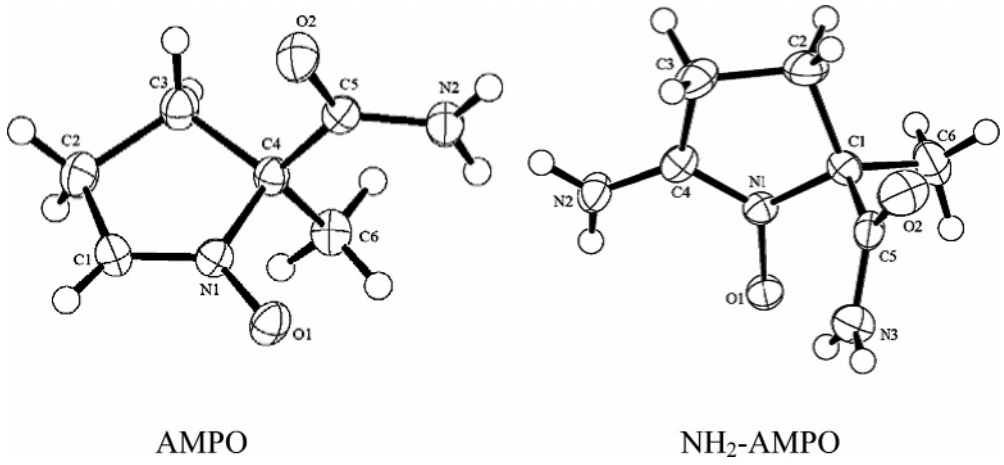

AMPO NH_2-AMPO

FIGURE 3. A view of the X-ray structure of AMPO (left) and NH_2−AMPO (right). The non-hydrogen atoms are drawn with 50% probability displacement ellipsoids. The hydrogen atoms are drawn with an arbitrary radius.

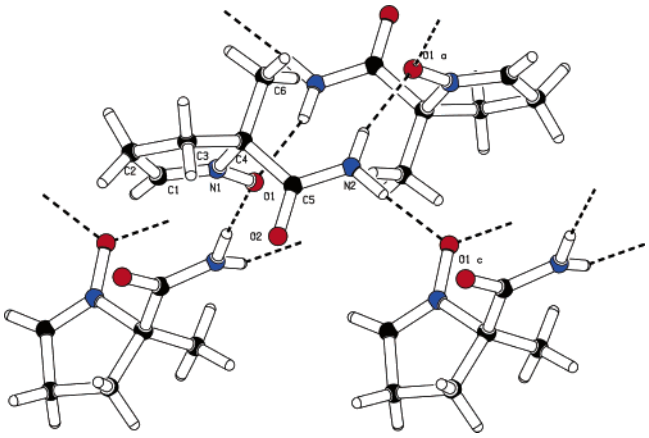

FIGURE 4. A view of the X-ray structure of AMPO showing the intermolecular H-bonding interaction between the amido-H and the nitronyl-O.

G, and $a_{\gamma-H}$ = 1.75 G. The theoretically predicted hfsc with use of eq 1 indicates that additional hfsc could result from the amide N, i.e., the calculated hfsc's for the most stable AMPO-O_2H *cis*-2a are $a_{nitronyl-N}$ = 12.53 G, $a_{amido-N}$ = 1.86 G, and $a_{\beta-H}$ = 14.53 G (Table S17). However, we could not make these assignments consistent with the experimentally obtained spectrum of the ^{15}N-labeled amide nitrogen of AMPO−OOH, or the relatively large hfsc due to amide N cannot be observed in the unlabeled AMPO−OOH. It should be noted, however, that these calculated a_X values do not account for the solvation effect and could still vary significantly after the environmental effects are considered.[33] Gas-phase calculations of the isotropic hyperfine splitting constants were also predicted for the most stable $O_2^{\bullet-}$ adducts of DMPO, EMPO, and DEPMPO, and gave good agreement with their experimental values in the aqueous phase (see Table S17).

The AMPO−O_2H showed slow decomposition to the corresponding OH (Figure 5a for the OH adduct) unlike the DMPO−O_2H.[34] Figure 2 shows a comparison of $O_2^{\bullet-}$ adducts of EMPO and DEPMPO and 1 h after their formation. Both EMPO−O_2H and DEPMPO−O_2H gave characteristic spectra (Figure 2a,b); however, their spectral profiles (Figure 2c,d) become obscure after 1 h due to their partial decomposition to the $^{\bullet}$OH adducts as well. Figure 2, spectra e and f, show the spectra of the independently generated $^{\bullet}$OH adducts and exhibit close resemblance to the partially decomposed $O_2^{\bullet-}$ adduct's spectra (Figure 2c,d). One probable advantage of AMPO−O_2H is that although it decomposes relatively slow to the OH adduct, its spectrum is uniquely different from its $^{\bullet}$OH adduct spectrum so that even in low concentrations, the AMPO−O_2H spectrum could not be misinterpreted as an $^{\bullet}$OH adduct. As demonstrated in Figure 7, the AMPO stability and its spin trapping characteristic were assessed in biological milieu by using PMA activated neutrophils and showed a distinguishable AMPO−O_2H spectrum over a period of 1 h. The presence of a characteristic signature for a "C-centered adduct" is evident during spin trapping by AMPO, using enzymatically generated $O_2^{\bullet-}$ (Figures 6a and 7), and is more evident with use of the light-riboflavin superoxide generating system (Figure 6c). Despite all attempts to obtain a more purified AMPO (as indicated by our spectroscopic data) as well as subjecting the finely ground sample to heating at 40 °C and 1 mmHg for 16 h, the spectra did not reflect the formation of the "C-centered adduct". Moreover, using the same experimental conditions for DMPO and DEPMPO did not yield such "C-centered adducts". The presence of a C-centered spectrum may be a result of other spin-trapping processes simultaneously occurring in solution or from an unidentified form of $O_2^{\bullet-}$ adduct that is in equilibrium with AMPO−O_2H, or its paramagnetic decomposition product.

Spin Adduct Stability. The lowest field peak intensity of the nitrone-O_2H spectrum was monitored, and no signal was observed before irradiation. However, peak formation does occur when the light source was turned on. Peak intensity begins to rise as a function of time and reaches a plateau over a certain period of time, then decreases when the light source is turned off. Decay plots (Figure 8) of the $O_2^{\bullet-}$ adducts were fitted by using eq 2, since fitting with a pure first or second order shows deviation from linearity. Therefore parallel first- and-

(33) Improta, R.; Barone, V. *Chem. Rev.* **2004**, *104*, 1231−1253.
(34) Buettner, G. R.; Oberley, L. W. *Biochem. Biophys. Res. Commun.* **1978**, *83*, 69−74.

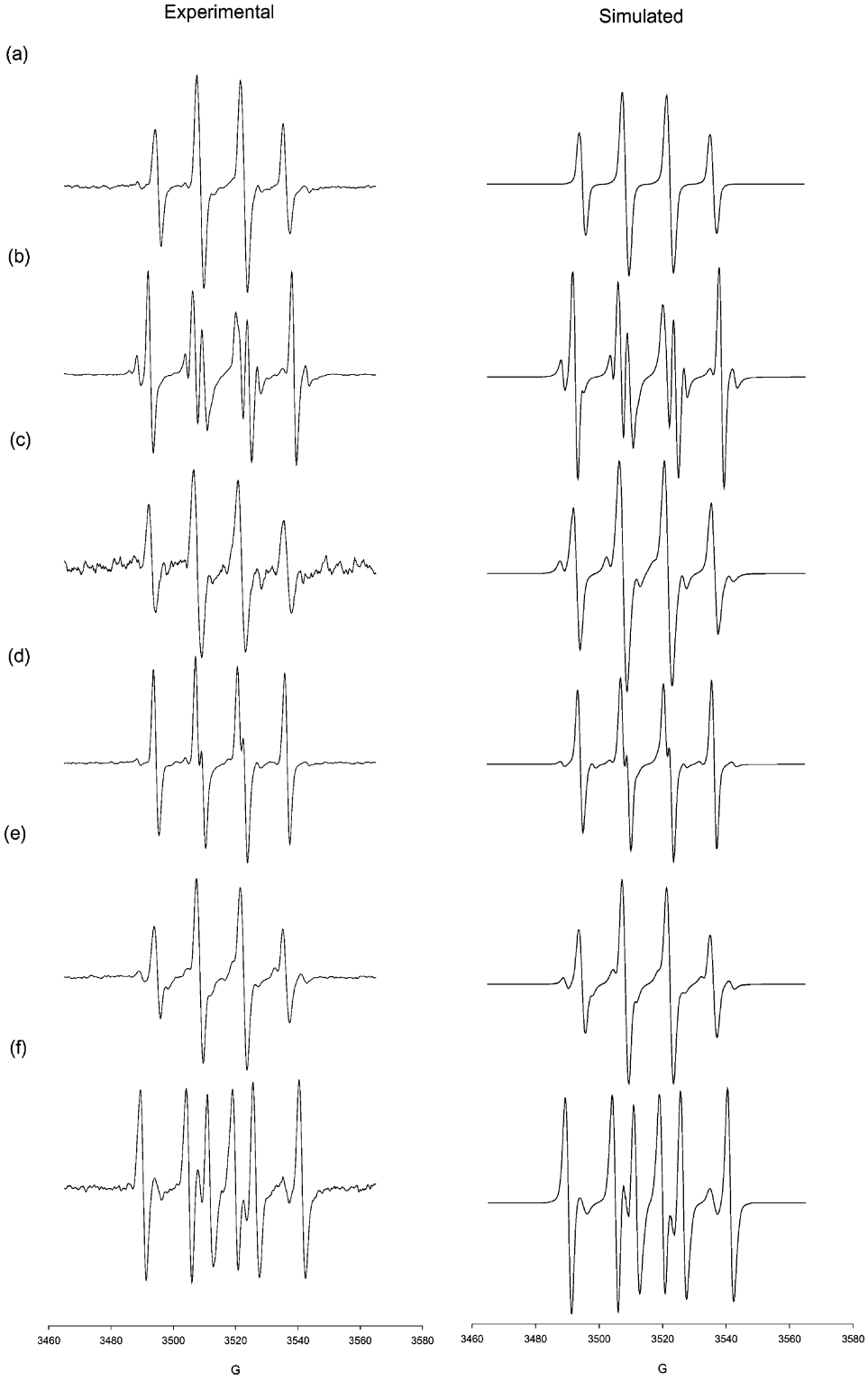

FIGURE 5. Experimental (left) and simulated (right) EPR spectra of AMPO radical adducts with (a) $^{\bullet}OH$, (b) $CO_2^{\bullet-}$, (c) $GS^{\bullet}$, (d) $SO_3^{\bullet-}$, (e) t-$BuO^{\bullet}$, and (f) $CH_3{}^{\bullet}CHOH$. See experimental methods for radical generation and spectrometer settings.

second-order reactions with a differential rate equation

$$-\frac{d[RA]}{dt} = k_1[RA] + 2k_2[RA]^2 \qquad (2)$$

was employed, where [RA] is the concentration of nitrone$-O_2H$, while k_1 and k_2 are the first- and second-order rate constants, respectively. A coefficient of 2 was included in the second-order expression to avoid ambiguity and to denote that two nitrone$-O_2$Hs undergo adisproportionation reaction. Half-lives of the $O_2^{\bullet-}$ adducts were approximated from the first-order rate constant and are shown in Table 3. Results show that the half-lives of AMPO$-O_2H$ ($t_{1/2} \sim 8$ min) and EMPO$-O_2H$ ($t_{1/2} \sim 10$

TABLE 2. EPR Parameters of Simulated Radical Adducts of AMPO[a]

radicals	generating system	diastereomers (%)	hyperfine coupling constants (G) a_N	a_{H^β}	a_{H^γ}
$O_2^{\bullet-}$	HX/XO[g]	80	13.0	10.8	
		20	13.1	12.5	1.75
$^\bullet OH$	$Fe^{2+}-H_2O_2$	69	14.0	13.5	
		31	14.0	12.5	
$CO_2^{\bullet-}$ [b]	$Fe^{2+}-H_2O_2-NaHCO_2$	47	14.25	18.15	
		53	14.53	16.48	
$SO_3^{\bullet-}$ [c]	$Fe^{2+}-H_2O_2-Na_2SO_3$	46	13.47	15.93	
		54	13.47	14.67	
$CH_3^\bullet CHOH$[d]	$Fe^{2+}-H_2O_2-EtOH$	100	14.8	21.4	
$(CH_3)_3CO^\bullet$ [e]	$(CH_3)_3COOC(CH_3)_3$	56	14.19	13.64	
	UV	44	13.85	12.79	
$GS^\bullet$ [f]	GSSG−UV	90	14.26	14.96	
		10	14.39	12.06	

[a] Based on the simulation program by Rockenbauer et al.[35] [b] Simulated spectrum contains 19% C-centered adduct and 12% OH adduct. [c] Simulated spectrum contains 23% C-centered adduct. [d] Simulated spectrum contains 13% OH adduct. [e] Simulated spectrum contains 10% C-centered adduct and 12% OOH-like adduct. [f] Simulated spectrum contains 12% C-centered adduct. [g] Hypoxanthine/xanthine oxidase.

min) are similar to the literature value of $t_{1/2} = 8$ min[36] or 8.6 min[14] for EMPO−O_2H. The AMPO−O_2H half-life of 8 min is relatively shorter compared to that found for DEPMPO−O_2H of $t_{1/2} = 16$ min but much longer than that of DMPO−O_2H of $t_{1/2} \sim 1$ min.

Partition Coefficient. Values obtained in this study (Table 3) are within an order of magnitude of those previously reported of 0.06,[31] 0.15,[14] and 0.1[37] for DEPMPO, EMPO, and DMPO, respectively. The partition coefficient value obtained for AMPO is similar to K_p values observed for most of the DMPO-type nitrones. Due to this similarity in K_p values, it is expected that permeability of AMPO through lipid bilayer membranes would be similar to that of DMPO and DEPMPO reported by Anzai et al.[38]

Experimental Section

2-Amino-5-carbamoyl-5-methyl-1-pyrroline *N*-Oxide (NH_2−AMPO). NH_2−AMPO was prepared by using the procedure described previously[39] with cyanide as catalyst for the aminolysis of esters. A solution of 100 mg (0.584 mmol) of EMPO in 25 mL of ca. 12 N NH_3 in MeOH and 28 mg (0.058 mmol) of NaCN was heated to 60 °C in a sealed tube for 40 h. The solvent was evaporated and the residue was redissolved in CH_2Cl_2. The organic phase was extracted with a minimal amount of water and dried over $MgSO_4$. Evaporation of the solvent gave a mixture of AMPO and NH_2−AMPO. The crude product was purifed by column chromatography, using silica gel and methanol−ethyl acetate (30:70) as solvent. The product was further purified twice by column chromatography with EtOH as solvent, which afforded NH_2−AMPO (5 mg), mp >200 dec. ^{1}H NMR (400 MHz, D_2O, 4.58 ppm) δ 1.40 (3 H, s, C(5)-Me), 1.90−2.06 and 2.22−2.35 (2 H, m, C(4)H), 2.59−2.65 (2 H, m, C(3)H). IR (neat film) 3346 and 1661 (N−H), 1682 (C=O), 1627 (C=N), 1201 (N−O). ESI-MS calcd for $C_6H_{11}N_3O_2Na^+$ *m/z* 180.0749, found 180.0743 amu.

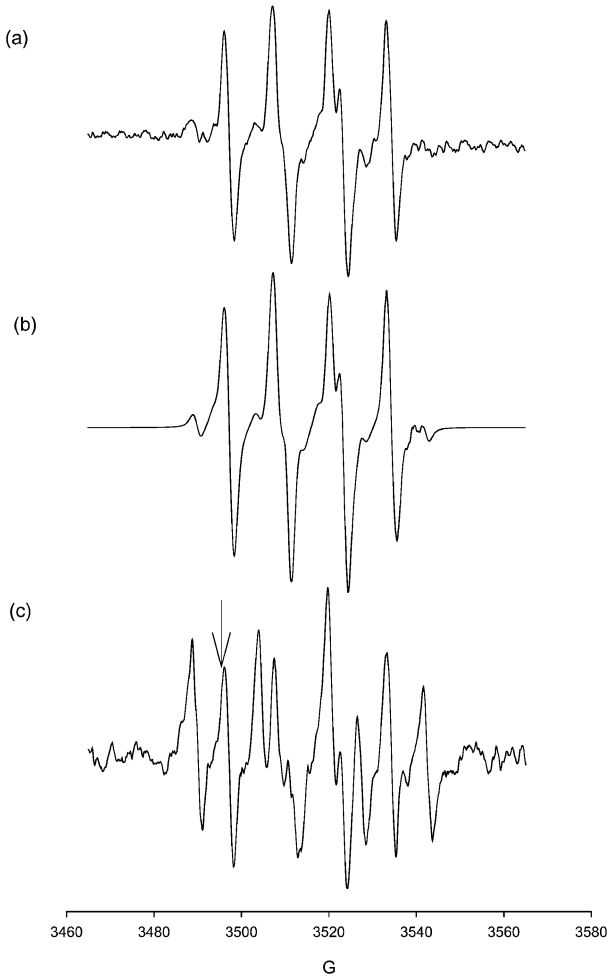

FIGURE 6. EPR spectral profile of AMPO−O_2H (a) generated by xanthine−xanthine oxidase; (b) simulated spectrum based on the parameters described in Table 2; (c) spectrum generated by the light-riboflavin system (note the significant contribution from a C-centered adduct). See experimental methods for spectrometer settings. The arrow indicates the peak being monitored during kinetic studies.

EPR Measurements. EPR measurements were carried out on an X band spectrometer with HS resonator at room temperature. General instrument settings are as follows unless otherwise noted: microwave power, 10 mW; modulation amplitutude, 1.0 G; receiver gain $3.17-3.56 \times 10^5$; for field sweep the scan time was 40 s and the time constant was 328 ms; for kinetic measurements at fixed magnetic field, the acquisition time was 335−2680 s and the time constant was 1310 ms. All spin-trapping studies were carried out in phosphate buffered saline containing 0.1 mM diethylenetriaminepentaacetic acid (DTPA). The total volume of all solutions used for EPR measurement was 50 μL, which was loaded into 50-μL micropipets. Samples were irradiated with a 150-W light source positioned 5 cm away from the sample cavity.

Decay Kinetics. In a typical decay kinetic study, 50 μL of solution containing 25 mM of the nitrone and 100 μM riboflavin was irradiated for 3 min in the cavity. The lowest field peak decay was monitored as a function of time over a period of 2680 s after the light source was turned off. All data were the average of three or more measurements.

Miscellaneous Spin-Trapping Studies. (a) Fenton Reaction System. A 50-μL 0.1 M phosphate buffer solution

(35) Rockenbauer, A.; Korecz, L. *Appl. Magn. Reson.* **1996**, *10*, 29−43.
(36) Zhang, H.; Joseph, J.; Vasquez-Vivar, J.; Karoui, H.; Nsanzumuhire, C.; Martasek, P.; Tordo, P.; Kalyanaraman, B. *FEBS Lett.* **2000**, *473*, 58−62.
(37) Janzen, E. G.; West, M. S.; Kotake, Y.; DuBose, C. M. *J. Biochem. Biophys. Methods* **1996**, *32*, 183−190.
(38) Anzai, K.; Aikawa, T.; Furukawa, Y.; Matsushima, Y.; Urano, S.; Ozawa, T. *Arch. Biochem. Biophys.* **2003**, *415*, 251−256.
(39) Hogberg, T.; Strom, P.; Ebner, M.; Ramsby, S. *J. Org. Chem.* **1987**, *52*, 2033−2036.

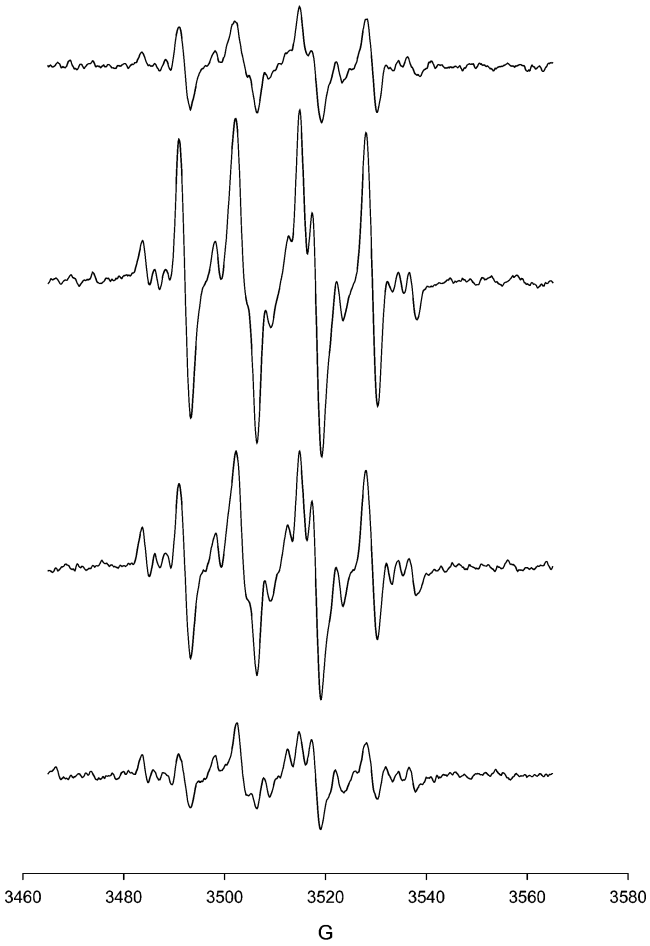

FIGURE 7. Superoxide adduct formation by 25 mM AMPO, using PMA-activated neutrophils: top to bottom 2, 10, 30, 60 min after the addition of PMA.

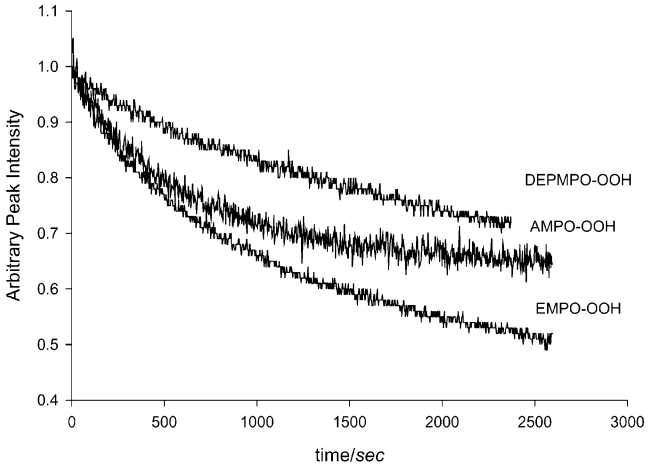

FIGURE 8. Decay plots of $O_2^{\bullet-}$ adducts of DEPMPO, EMPO, and AMPO after 3 min of visible light irradiation of solutions containing 25 mM of the corresponding nitrone and 100 μM riboflavin in pH 7.2 phosphate buffer.

containing 30 mM AMPO, 1% H_2O_2, and 65 mM $FeSO_4$ was transferred to a 50-μL capillary tube and the EPR spectrum of the hydroxyl adduct was recorded over a 5 min time period.

(b) Trapping of $SO_3^{\bullet-}$, $CO_2^{\bullet-}$, and $CH_3^{\bullet}CHOH$ Radicals. A 50-μL 0.1 M phosphate buffer solution containing 30 mM AMPO, 1% H_2O_2, and 100 mM of the respective radical source

TABLE 3. First-Order Approximation Half-Lives of Nitrone−Superoxide Adducts and Partition Coefficient of the Nitrone Spin Traps at pH 7.2 and 23 °C

spin trap	$k_1/10^{-4}$ s^{-1}	$t_{1/2}$/min[a]	ref	K_p(*n*-octanol/water)[b]
AMPO	14.0 ± 1.2	8.3 ± 0.7	this work	0.03
EMPO	11.6 ± 0.5	9.9 ± 0.4	this work	0.33
		8.6	14	
		8.0	36	
		24.6 ± 2.7	18	
DEPMPO	7.5 ± 0.7	15.5 ± 1.4	this work	0.16
	8.13	14.2	16	
DMPO	129.0	0.9	16	0.06

[a] Based on the first-order rate constant; values are the mean average of 3−6 measurements. [b] Shaken for 2 h at 37 °C.

$NaHCO_2$, Na_2SO_3, or ethanol was prepared with 65 mM freshly prepared $FeSO_4$. The mixture was then transferred to a 50-μL capillary tube and the EPR spectrum of the adduct was recorded over a 5 min time period.

(c) Trapping of GS$^{\bullet}$ and *t*-BuO$^{\bullet}$ Radicals. A 50-μL 0.1 M phosphate buffer solution containing 30 mM AMPO and 100 mM GSSG or $(CH_3)_3CO-OC(CH_3)_3$ was prepared. The mixture was then transferred to a 50-μL capillary tube and the radicals were generated by UV photolysis. The EPR spectrum of the adduct was recorded over a 5 min time period.

(d) Trapping of $O_2^{\bullet-}$. Typical $O_2^{\bullet-}$ trapping experiments utilized the riboflavin-light system as previously described.[16] An alternative $O_2^{\bullet-}$ generating system used a solution of 0.4 mM hypoxanthine and 0.5 unit/mL xanthine oxidase, or 10 nM PMA and 8 × 10^5 neutrophil cells in 25 mM AMPO. Spectra were acquired over a period of 15 min.

Partition Coefficient. To a 100-μL aqueous solution of 400 mM nitrone was added 100 μL of *n*-octanol. The mixture was vigorously mixed for 2 h at 37 °C and centrifuged. The concentration of the nitrones was analyzed by using a UV−vis spectrophotometer. Standard curves were constructed for each of the nitrones at wavelengths of 226 nm for DMPO and EMPO, 233 nm for DEPMPO, and 230 nm for AMPO. The concentration of the nitrone in the organic phase was determined by subtracting the original concentration of the nitrone from the concentration in the aqueous layer after vigorous mixing. Partition coefficient K_p is expressed as $[\text{nitrone}]_{n-\text{octanol}}/[\text{nitrone}]_{\text{buffer}}$.

Computational Methods. Density functional theory[40,41] was applied in this study to determine the optimized geometry, vibrational frequencies, and single-point energy of all stationary points.[42−45] The effect of solvation on the gaseous phase calculations was also investigated by using the polarized continuum model (PCM).[46−49] All calculations were performed with Gaussian 98[50] at the Ohio Supercomputer Center. Single-point energies were obtained at the B3LYP/6-31+G** level based on the optimized B3LYP/6-31G* geometries. Stationary points for both the nitrone spin traps and spin adducts have no imaginary vibrational frequencies as derived from a vibrational frequency analysis (B3LYP/6-31G*). A scaling factor of

(40) Labanowski, J. W.; Andzelm, J. *Density Functional Methods in Chemistry*; Springer: New York, 1991.
(41) Parr, R. G.; Yang, W. *Density Functional Theory in Atoms and Molecules*; Oxford University Press: New York, 1989.
(42) Becke, A. D. *Phys. Rev. A* **1988**, *38*, 3098.
(43) Becke, A. D. *J. Chem. Phys.* **1993**, *98*, 5648.
(44) Lee, C.; Yang, W.; Parr, R. G. *Phys. Rev. B* **1988**, *37*, 785.
(45) Hehre, W. J.; Radom, L.; Schleyer, P. V.; Pople, J. A. *Ab Initio Molecular Orbital Theory*; John Wiley & Sons: New York, 1986.
(46) Barone, V.; Cossi, M.; Tomasi, J. *J. Chem. Phys.* **1997**, *107*, 3210.
(47) Barone, V.; Cossi, M.; Tomasi, J. *J. Comput. Chem.* **1998**, *19*, 404.
(48) Cossi, M.; Barone, V.; Cammi, R.; Tomasi, J. *Chem. Phys. Lett.* **1996**, *255*, 327.
(49) Tomasi, J.; Persico, M. *Chem. Rev.* **1994**, *94*, 2027.

0.9806 was used[51] for the zero-point vibrational energy (ZPE) corrections. Spin contamination for all of the stationary points for the spin adduct radical structures was negligible, i.e., $0.75 < \langle S^2 \rangle < 0.76$. All spin and charge densities were obtained from natural population analyses (NPA) at the B3LYP/6-31G* level.[52]

Crystallographic Structure. Single crystals of AMPO were obtained from slow evaporation at room temperature of its solution in methanol−benzene. The data collection crystal for AMPO was a thin colorless plate. Examination of the diffraction pattern on a CCD diffractometer indicated a monoclinic crystal system. All work was done at 200 K. The data collection strategy was set up to measure a quadrant of reciprocal space with a redundancy factor of 3.1, which means that 90% of the reflections were measured at least 3.1 times. A combination of phi and omega scans with a frame width of 2.0° was used. Data integration was done with Denzo,[53] and scaling and merging of the data was done with Scalepack.[53] Merging the data and averaging the symmetry equivalent reflections resulted in an R_{int} value of 0.044. The structure was solved by direct methods in SHELXS-86.[54] Full-matrix least-squares refinements based on F^2 were performed in SHELXL-93.[55]

A pale yellow approximately rectangular plate single crystal of NH_2−AMPO was obtained similar to the procedure described for AMPO but with methylene chloride−ethyl acetate as solvents. The diffraction pattern on a CCD diffractometer indicated an orthorhombic crystal system. The data collection strategy was set up to measure an octant of reciprocal space with a redundancy factor of 4.4. The teXsan[56] package indicated the space group to be P 2(1)2(1)2(1).

Full details of the crystallographic data for AMPO and NH_2−AMPO are described in the Supporting Information (S17−S34).

Conclusion

The spin-trapping properties of AMPO have been demonstrated for the first time. AMPO is a solid spin trap that is easy to purify without giving paramagnetic impurities based on its EPR spectrum. The nitrone AMPO exhibited characteristic EPR spectra with various radicals, notably, $O_2^{\bullet-}$ vs $^{\bullet}OH$ adduct. Optimized geometry calculations for AMPO and its $O_2^{\bullet-}$ adduct show evidence of intramolecular H-bonding. The most plausible mechanism for AMPO−O_2H formation based on the calculated thermodynamic data is the addition of $O_2^{\bullet-}$ to AMPO to form the anionic adduct AMPO−O_2^-, and subsequent protonation giving the hydroperoxyl adduct, AMPO−O_2H. An X-ray structure determination of the analogous NH_2−AMPO further supports the calculated structural features of AMPO. The half-life of the AMPO−O_2H is comparable to that of EMPO−O_2H but shorter compared to that of DEPMPO−O_2H. Thermodynamic properties of superoxide radical addition to nitrones can predict favorable formation of certain adducts. The partition coefficient K_p of AMPO is comparable for all nitrones investigated in this study. This study, therefore, demonstrates the suitability of AMPO as a spin trap to study radical production in aqueous systems.

Acknowledgment. The authors wish to thank Prof. David Hart of the OSU Chemistry Department and Prof. DeLanson R. Crist of the Georgetown University Chemistry Department for helpful discussions. The Ohio Supercomputer Center (OSC) is acknowledged for support of this research. This work was supported by NIH grants HL38324, HL63744, and HL65608. C.M.H. acknowledges support from the NSF-funded Environmental Molecular Science Institute (CHE-0089147). A.R. acknowledges support from the Hungarian Scientific Research Fund OTKA T-046953.

Supporting Information Available: Energies, enthalpies, and free energies for all spin traps and their corresponding adducts as well as ^{1}H NMR, IR, and MS spectra. This material is available free of charge via the Internet at http://pubs.acs.org.

JO049244I

(50) Frisch, M. J.; Trucks, G. W.; Schlegel, H. B.; Scuseria, G. E.; Robb, M. A.; Cheeseman, J. R.; Zakrzewski, V. G.; Montgomery, J. A., Jr.; Stratmann, R. E.; Burant, J. C.; Dapprich, S.; Millam, J. M.; Daniels, A. D.; Kudin, K. N.; Strain, M. C.; Farkas, O.; Tomasi, J.; Barone, V.; Cossi, M.; Cammi, R.; Mennucci, B.; Pomelli, C.; Adamo, C.; Clifford, S.; Ochterski, J.; Petersson, G. A.; Ayala, P. Y.; Cui, Q.; Morokuma, K.; Malick, D. K.; Rabuck, A. D.; Raghavachari, K.; Foresman, J. B.; Cioslowski, J.; Ortiz, J. V.; Stefanov, B. B.; Liu, G.; Liashenko, A.; Piskorz, P.; Komaromi, I.; Gomperts, R.; Martin, R. L.; Fox, D. J.; Keith, T.; Al-Laham, M. A.; Peng, C. Y.; Nanayakkara, A.; Gonzalez, C.; Challacombe, M.; Gill, P. M. W.; Johnson, B. G.; Chen, W.; Wong, M. W.; Andres, J. L.; Head-Gordon, M.; Replogle, E. S.; Pople, J. A. *Gaussian 98*, revision A.11.3; Gaussian, Inc.: Pittsburgh, PA, 1998.

(51) Scott, A. P.; Radom, L. *J. Phys. Chem.* **1996**, *100*, 16502−16513.

(52) Reed, A. E.; Weinhold, F. A.; Curtiss, L. A. *Chem. Rev.* **1998**, *98*, 899.

(53) Otwinowski, Z.; Minor, W. In *Macromolecular Crystallography*, *Part A in Methods in Enzymology*; Carter, C. W., Jr., Sweet, R. M., Eds.; Academic Press: New York, 1997; Vol. 276, pp 307−326.

(54) *SHELXS-86*: Sheldrick, G. M. *Acta Crystallogr.* **1990**, *A46*, 467−473.

(55) *SHELXL-93*: Sheldrick, G. M. Universitat Gottingen, Germany 1993.

(56) *teXsan*, version 1.7−2: Crystal Structure Analysis Package; Molecular Structure Corporation: Woodlands, TX, 1995.